# Retrieval and Classification of Pneumoconiosis Chest Radiograph Images Using Multiscale AM-FM Methods

Victor Murray*, Marios Pattichis* and Peter Soliz†
*University of New Mexico, Department of Elect. and Comp. Eng., Albuquerque, New Mexico, U.S.A.
†VisionQuest Biomedical, Albuquerque, New Mexico, U.S.A.
E-mails: vmurray@ieee.org, pattichis@ece.unm.edu, psoliz@visionquest-bio.com

***Abstract*—We propose the use of Amplitude-Modulation Frequency-Modulation (AM-FM) features for representing and retrieving X-Ray images with pneumoconiosis. The AM-FM features are estimated using multiscale filterbanks with wavelengths related with the standard sizes for grading the level of opacities in X-Rays. The extracted AM-FM features represent opacity profusion in terms of instantaneous frequency (IF) and instantaneous amplitude (IA) features. Here, IF estimates in the medium and high scale frequencies can be used to capture early disease symptoms. AM-FM features from the low and medium scale frequencies are associated with advanced disease stages. We demonstrate the performance of the system in X-ray image retrieval and classification applications.**

***Index Terms*—AM-FM, X-ray chest imaging**

## I. Introduction

Chest radiograph images are used in the screening, surveillance, and diagnosis of dust-related respiratory illness resulting from silica and coal dust, asbestos, and a variety of other dusts. In clinical practice, the International Labor Organization (ILO, [1]) standards are used for interpreting the chest radiograph images for inorganic dust-induced diseases or pneumoconioses.

The US remains 6th in the world for pneumoconiosis and interstitial lung disease (ILD) or pulmonary interstitial fibrosis as large numbers of workers continue to be exposed to dust in their work environment. Coal workers' pneumoconiosis (CWP) is identified by a specific pattern of X-Ray abnormalities and a history of exposure to coal dust. The chest radiograph is the single most useful tool for clinically evaluating both occupationally related and non-occupational chronic lung diseases.

Early work on X-ray image retrieval includes the work by Hasegawa et. al. [2] based on sketches. Earlier work in analyzing Pneumoconiosis image analysis also includes the use of binarized images with Neural Networks to detect opacities [3], [4] and the use of spatial gray level dependence matrices (SGLDM) and gray level difference statistics (GLDS) with different classifiers for classifying regions of interest [5]. A recent review of content-based image retrieval applications can be found in [6].

In [7], we presented earlier results for classifying chest radiographs using AM-FM multiscale methods with adapted filterbanks on a limited database. In this paper, we extend this research into an image retrieval system using a two-step classifier followed by the use of a distance metric to rank the retrieved chest radiographs. We test our method over an extended database.

The method is based on a new multi-scale Amplitude-Modulation Frequency-Modulation (AM-FM) approach [8], [9]. Images are analyzed over a dyadic filter-bank and AM-FM image features are extracted from different scales. For each pixel, we obtain dominant instantaneous frequency (IF) and instantaneous amplitude (IA) estimates that are used for classification and retrieval.

We summarize the methodology in section II. Results are given in section III and a discussion is given in section IV. We have concluding remarks in section V.

## II. Methodology

### A. Database Used

Two image databases were used: (i) a database from the Miners' Colfax Medical Center and the Grant's Uranium Miners, Raton, New Mexico, and (ii) a second database from the National Institute for Occupational Safety and Health (NIOSH) Standards. To improve the contrast of the digitized X-Ray images, we applied a logarithmic transformation to the images [10]. For each input image $I(\cdot)$, we produce an image $I_n(\cdot)$ such that $I_n(\cdot) = \log_{10}(1 + 10^n I(\cdot))$. For our database, we used the fixed value of $n = -2$ to improve the visual display of the images (see [10] for details).

*1) Database 1: Raton - New Mexico:* The database consists of chest radiographs taken from miners from the Miners' Colfax Medical Center and the Grant's Uranium Miners, Raton, New Mexico. We use 11 X-Ray images from different patients, graded according to the ILO standard for profusion of opacities: (i) 4 patients in category 0/0, (ii) 4 patients in category $1/1$ and (iii) 3 patients in category $2/2$, where $0/0$ is no signs of opacities and progressively more profusion from $1/1$ to $2/2$. Each X-Ray image is $4200 \times 5100$ pixels and digitized in uncompressed TIF format at 300 dpi resolution. We performed a simple, automatic segmentation of both right and left lungs based on maximum intensity projection along the columns. Each segmented region is $1600 \times 1400$ pixels per lung and covers the upper region of the lung.

*2) Database 2: NIOSH Standards:* The National Institute for Occupational Safety and Health's X-Ray images are graded according to the ILO standard for profusion of opacities: (i) 1 case of $0/0$, (ii) 9 cases of $1/1$ and (iii) 1 case of $2/2$. Type *qq* of opacities are present (see [1]). Each X-Ray image is $4194 \times 4321$ pixels and digitized in uncompressed TIF format at 300 dpi resolution. The segmentation method applied to this database is similar to the one described in the previous subsection II-A2.

### B. AM-FM Methods

We consider multi-scale AM-FM representation of digital non-stationary images given by [9], [11], [12]

$$I(k_1, k_2) \approx \sum_{n=1}^{M} a_n(k_1, k_2) \cos \varphi_n(k_1, k_2), \qquad (1)$$

where $n = 1, 2, \ldots, M$ denote different scales, $a_n(k_1, k_2)$ denotes slowly-varying instantaneous amplitude (IA) function and $\varphi_n(k_1, k_2)$ denotes the instantaneous phase (IP) functions. The basic idea is to let the frequency-modulated (FM) components $\cos \varphi_n(k_1, k_2)$ capture fast-changing spatial variability in the image intensity. The instantaneous frequency (IF) $\nabla \varphi_n(k_1, k_2)$ is defined in terms of the gradient of the IP: $\nabla \varphi_n(k_1, k_2) = (\partial \varphi_n / \partial k_1(k_1, k_2),\, \partial \varphi_n / \partial k_2(k_1, k_2))$.

For a single-scale AM-FM representation ($M = 1$ in (1)), the IA and the IP are estimated using [13] $\hat{a}(k_1, k_2) = |\hat{I}_{AS}(k_1, k_2)|$ and $\hat{\varphi}(k_1, k_2) = \arctan\left(\text{imag}(\hat{I}_{AS}(k_1, k_2)) / \text{real}(\hat{I}_{AS}(k_1, k_2))\right)$, respectively, with $\hat{I}_{AS}(k_1, k_2) = I(k_1, k_2) + j\mathcal{H}_{2d}[I(k_1, k_2)]$, where $\mathcal{H}_{2d}$ denotes a two-dimensional extension of the one-dimensional Hilbert transform operator. For robust IA and IF estimations, we use a variable spacing, local linear phase (VS-LLP) method as described in [9], [11]. Here, for estimating the first component, we generate four estimates using:

$$\hat{\varphi_1}(k_1, k_2) = \frac{1}{n_1} \arccos\left(\frac{\bar{I}_{AS}(k_1 + n_1, k_2) + \bar{I}_{AS}(k_1 - n_1, k_2)}{2\bar{I}_{AS}(k_1, k_2)}\right), \qquad (2)$$

where $\bar{I}_{AS}(k_1, k_2) = \hat{I}_{AS}(k_1, k_2)/|\hat{I}_{AS}(k_1, k_2)|$, $n_1$ represents a variable displacement, from 1 to 4. VS-LLP produces the most accurate of the four estimates by considering the condition number of the $\arccos(\cdot)$ function [9], [11]. The approach is similar for the second component direction.

### C. Multi-scale filterbank

Here, we consider a multi-scale approach developed by Murray and Pattichis that uses AM-FM components extracted from different scales [9], [11]. We define the scales using a collection of bandpass filters as follows: (i) LPF (lowpass filter), (ii) VL (very low frequencies), (iii) L (low frequencies), (iv) M (medium frequencies) and (v) H (high frequencies) as given in [9]. For the opacities problem, we consider eleven different combinations of scales for extracting the dominant AM-FM estimates (see Table I). From each combination of scales, we extract the histograms of the IA, the IF magnitude (|IF|), and the IF angle.

The motivation behind the use of scales and filter-banks is due to variability of the underlying image structures. With the knowledge of the sizes, we can relate the lengths with the corresponding frequencies. The resulting cut-off frequencies are presented in [7].

### D. Histograms processing

The AM-FM estimates from each image are encoded by producing their histograms. For each of the 11 CoS (see Table I), we create a 96-bin feature vector that contains the AM-FM histograms. Each AM-FM histogram has the information of (32-bin each): (i) the IA, (ii) the IF magnitude and (iii) the IF angle. Thus, each image produces 11 different feature vectors, each one corresponding to one of the 11 different CoS.

Since the AM-FM estimates of contiguous pixels could have the problem of noisy estimates, a $9 \times 9$ median filter is applied to the output of the IA and IF estimates (see [9], [11], [14]). This filtering produces a continuous estimation in the sense of the selection of the dominant component over the bandpass filters.

Due to the ambiguity of the instantaneous frequency vectors (coming from $\cos \varphi(k_1, k_2) = \cos(-\varphi(k_1, k_2))$), we map the IF estimates to two frequency quadrants:

- Instantaneous frequencies $\frac{\partial \varphi_n}{\partial x}(x, y) \geq 0$ and $\frac{\partial \varphi_n}{\partial y}(x, y) \geq 0$ are kept as they are.
- Instantaneous frequencies $\frac{\partial \varphi_n}{\partial x}(x, y) \geq 0$ and $\frac{\partial \varphi_n}{\partial y}(x, y) < 0$ are kept as they are.
- Instantaneous frequencies $\frac{\partial \varphi_n}{\partial x}(x, y) < 0$ and $\frac{\partial \varphi_n}{\partial y}(x, y) < 0$ are mapped to $|\frac{\partial \varphi_n}{\partial x}(x, y)|$ and $|\frac{\partial \varphi_n}{\partial y}(x, y)|$.
- Instantaneous frequencies $\frac{\partial \varphi_n}{\partial x}(x, y) < 0$ and $\frac{\partial \varphi_n}{\partial y}(x, y) \geq 0$ are mapped to $|\frac{\partial \varphi_n}{\partial x}(x, y)|$ and $-|\frac{\partial \varphi_n}{\partial y}(x, y)|$.

Then, the IF histograms are computed.

For the IF angle, given by $\arctan\left(\frac{\partial \varphi_n}{\partial y}(x, y) / \frac{\partial \varphi_n}{\partial x}(x, y)\right)$, we center the histogram according to the maximum value as:

$[h] \leftarrow$ `histogram{IF angle using` $l$ `bins}`, {where $h$ is a column vector.}
$H \leftarrow [hhh]$, {triplicate version of $h$.}
$i \leftarrow$ `Location of the maximum value of` $h$.
$h \leftarrow H_{l+i-l/2+1:l+i+l/2}$.

As last step, all the computed histograms (IA, IF magnitude and IF angle) are normalized such that the cumulative sum of each one is equal to 1 (one).

### E. Partial Least Squares Classification

Partial Least Squares (PLS) is a linear regression method that is used to create a classifier using the AM-FM features extracted from medical images. The regression problem is setup using

$$y = X\beta + \varepsilon, \qquad (3)$$

TABLE I
COMBINATIONS OF SCALES (COS) USED FOR COMPUTING THE DOMINANT AM-FM FEATURE PARAMETERS.

| CoS | Scales used | CoS | Scales used |
|---|---|---|---|
| 1 | VL, L, M, H | 7 | LPF, VL |
| 2 | LPF | 8 | VL, L |
| 3 | VL | 9 | L, M |
| 4 | L | 10 | M, H |
| 5 | M | 11 | H |
| 6 | LPF, VL, L, M, H | | |

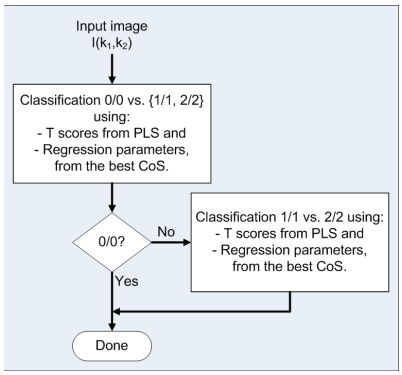


Fig. 1. Two-step classification flowchart. In the first processing block, we detect if the input image is normal (0/0) or abnormal. If the image is abnormal, the level of profusion (1/1 or 2/2)is determined in the second processing block.

where $y$ is a $n \times 1$ vector of dependent variables, $X$ is a $n \times p$ matrix of independent variables, $\beta$ is a $p \times 1$ vector of regression weights, and $\varepsilon$ is a $n \times 1$ vector of residuals. The least squares solution to estimating $\beta$ is given by the normal equations $\beta = (X^T X)^{-1}(X^T y)$.

When there are more variables than cases ($p > n$) or when the columns of $X$ are highly correlated (multi-colinearity), $X^T X$ will be singular or nearly singular and a unique solution to the normal equations does not exist. PLS is based on a reduction of $X$ to a lower dimensional subspace ($k \ll p$). The first step for both methods is to factor $X$ as $X = TL$, where $T$ is an orthogonal $n \times k$ matrix of $T$-scores and $L$ is a $k \times p$ matrix of factor loadings. The $T$-scores matrix can be used to find a threshold for a classifier.

We apply PLS to determine the optimal number of factors for each one of the eleven CoS from Table I. We then select the factors from the combinations of scales that gave the best results to form a joint feature matrix over all scales. We also select optimal factors from the joint feature matrix.

### *F. Two-step classification and retrieval table*

In Fig. 1 we show the flowchart for the two-step classification method implemented based on PLS. Using the T-scores from the previous subsection II-E, we first determine if the input image is normal (graded 0/0) or abnormal (1/1 or 2/2). If the image is abnormal, we apply the regression parameters from the training related to distinguish between grades 1/1 and 2/2. Note that for this results, we do not consider intermediate grades such as 1/2 or 2/1 (see [1]).

Once the chest X-Ray image has been classified, we produce a table of the distances among all the images within the same class using the reduced features from the T-scores. The Euclidean distance metric was used. Thus, the system finds the most similar images for an input query image.

## III. RESULTS

### *A. Image Retrieval and Classification using AM-FM methods*

We consider four classification problems: (i) profusion 0/0 versus 2/2, (ii) 0/0 versus 1/1, (iii) 1/1 versus 2/2 and (iv) normal versus abnormal (0/0 versus both 1/1 and 2/2 at the same time). In Table II we present the area under the receiver operator characteristics curve (AUC), in terms of specificity and sensitivity, with the corresponding number of latent factor used for each combination. In general, the less number of factors we use, the more robust the classification system. To improve the robustness of our method, we create a new feature vector per image that consists of the combination of the cases that produced the best AUC individually. The goal of this procedure is to improve the classification results combining the information of all images at different scales but only in frequency ranges where the information is important. The independent AUC computed for each case together with the number of factors used give us the best cases to use. For the classification we keep the cases that produced both an AUC bigger than 0.7 and with a number of factors $<0.5\times\{$Total Number of images used$\}$.

When the best CoS are used, for the four classification problems, a perfect classification is obtained (AUC = 1.0) using a total of 2 latent factors. We show the estimated values for each problem in Fig. 2.

### *B. Two-step classification results*

From the previous subsection III-A, it is clear that a perfect classification can be obtained using the reduced T-scores from the features vectors. For each classification problem, the best CoS are used. Once an input image is classified in either grade 0/0 or 1/1 or 2/2, the Euclidean distances among the images of the same grade is computed (see subsection II-F). We present in Fig. 3 an example for one image of each grade. Grades 0/0, 1/1 and 2/2 in rows 1, 2 and 3, respectively. In the first column we show the query image (after applying the logarithm transformation from subsection II-A) and then the retrieved images in ascendant order according to their distances.

## IV. DISCUSSION

From Table II, we note that the classification between categories 0/0 and 2/2 is the most clear. Indeed, CoS 10 performed the classification using only 2 factors with an AUC equal to 1. On the other hand, the classification between types normal and abnormal is the most difficult one. However, when we use the best combinations of scales together, a perfect classification is obtained and the number of factors is 2.

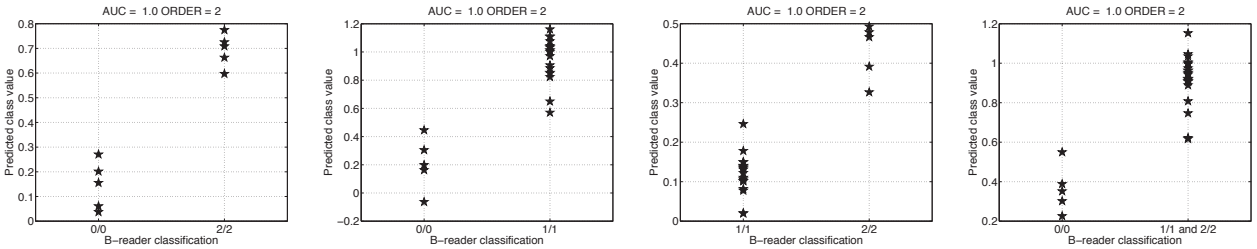


(a) (b) (c) (d)

Fig. 2. Results of the classification. (a) 0/0 vs. 2/2. (b) 0/0 vs. 1/1. (c) 1/1 vs. 2/2. (d) 0/0 vs. {1/1 and 2/2}.

TABLE II

AREA UNDER THE CURVE (AUC) FOR CLASSIFICATION OF THE X-RAY IMAGES, WITH ITS CORRESPONDING NUMBER OF FACTORS (ORDER), PRODUCED WHEN BY EACH COMBINATION INDEPENDENTLY. BEST RESULTS TO BE USED ARE SHOWN IN **BOLD** TYPEFACE. BEST RESULTS CRITERIA: (I) INDIVIDUAL AUC$>0.7$ AND (II) NUMBER OF FACTORS$<0.5\times\{$TOTAL NUMBER OF IMAGES USED$\}$

| | **Classification by categories** | | | | | | | |
|---|---|---|---|---|---|---|---|---|
| | **0/0 vs. 2/2** | | **0/0 vs. 1/1** | | **1/1 vs. 2/2** | | **0/0 vs. {1/1 & 2/2}** | |
| **CoS** | **AUC** | **Order** | **AUC** | **Order** | **AUC** | **Order** | **AUC** | **Order** |
| **1** | **1.00** | 4 | **0.92** | 7 | **0.88** | 4 | 0.98 | 17 |
| **2** | **0.76** | 4 | **0.91** | 2 | **0.81** | 8 | **0.92** | 10 |
| **3** | **0.80** | 3 | **0.94** | 4 | 0.89 | 22 | 0.91 | 27 |
| **4** | 0.80 | 7 | **0.94** | 5 | 0.88 | 22 | **0.91** | 6 |
| **5** | 0.80 | 6 | **0.79** | 4 | 0.63 | 3 | **0.71** | 9 |
| **6** | **0.76** | 4 | **0.91** | 2 | **0.81** | 8 | **0.92** | 10 |
| **7** | **0.76** | 4 | **0.91** | 2 | **0.81** | 8 | **0.92** | 10 |
| **8** | 0.84 | 9 | **0.92** | 5 | **0.79** | 6 | 0.92 | 16 |
| **9** | 1.00 | 6 | **0.96** | 11 | **0.70** | 4 | **0.94** | 4 |
| **10** | **1.00** | 2 | **0.91** | 2 | **0.98** | 6 | **0.92** | 4 |
| **11** | **1.00** | 3 | **0.96** | 5 | **0.99** | 6 | **0.95** | 4 |

The perfect classification results guarantees that the correct chest radiograph images are being retrieved. Unfortunately, due to our limited database, we could not yet assess the rankings produced by the use of Euclidean distances (within the retrieved images).

## V. CONCLUSIONS

We have developed a new multi-scale AM-FM classification system for retrieving chest radiographs. We have obtained perfect classification results for our limited database. The use of single combinations of scales could produce perfect classification (see AUC per case in Table II). The IF estimates computed in medium and high frequencies are able to detect the first symptoms and appearance of opacities in the chest. Values in the range of low and medium frequencies show to describe the different grades when the disease is in advanced stage. The use of the joint combination of the best scales produced only two factors for all the classification experiments.

This system produces better results than those presented in [5], [15]. Furthermore, the system has been expanded to produce a ranking of the classified images into an image retrieval system. Here, perfect classification guarantees that the retrieved images are related to the query image. Further research is necessary to assess the quality of the rankings of the retrieved images.

## REFERENCES

[1] International Labour Office, *Guidelines for the use of ILO International Classification of Radiographs of Pneumoconioses*, Geneva, Switzerland, 1980.

[2] J.-I. Hasegawa, N. Okada, and J.-I. Toriwaki, "Intelligent retrieval of chest x-ray image database using sketches," *Systems and Computers in Japan*, vol. 20, no. 7, pp. 29–42, 1989.

[3] H. Kondo and T. Kouda, "Computer-aided diagnosis for pneumoconiosis using neural network," in *IEEE Symposium on Computer-Based Medical Systems*, 26-27 July 2001, pp. 467–472.

[4] ——, "Detection of pneumoconiosis rounded opacities using neural network," in *Joint 9th IFSA World Congress and 20th NAFIPS International Conference*, vol. 3, 25-28 July 2001, pp. 1581–1585.

[5] M. Pattichis, C. Pattichis, C. Christodoulou, D. James, L. Ketai, and P. Soliz, "A screening system for the assessment of opacity profusion in chest radiographs of miners with pneumoconiosis," in *IEEE Southwest Symposium on Image Analysis and Interpretation*, 7-9 April 2002, pp. 130–133.

[6] T. M. Lehmann, M. O. Gold, C. Thies, B. Fischer, K. Spitzer, D. Keysers, H. Ney, M. Kohnen, H. Schubert, and B. B. Wein, "Content-based image retrieval in medical applications," *Methods of Information in Medicine*, vol. 43, pp. 354–361, 2004.

[7] V. Murray, M. S. Pattichis, H. Davis, E. S. Barriga, and P. Soliz, "Multiscale AM-FM analysis of pneumoconiosis x-ray images," in *IEEE International Conference on Image Processing*, 2009.

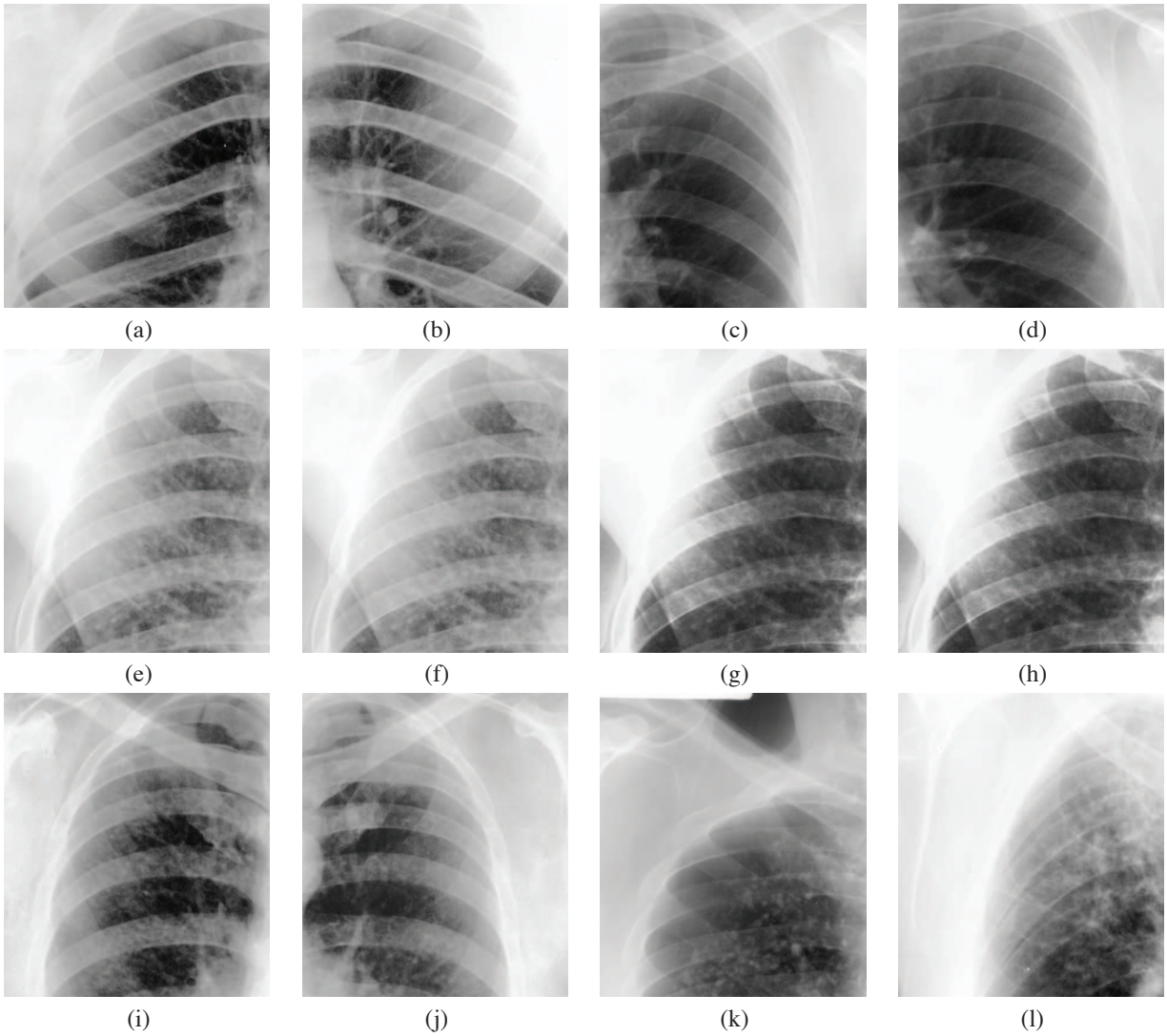


Fig. 3. Examples of retrieving the pneumoconiosis images. (a) Query 0/0 images. (b)-(d) Retrieved 0/0 images in ascendent order. (e) Query 1/1 images. (f)-(g) Retrieved 1/1 images in ascendent order. (i) Query 2/2 images. (j)-(l) Retrieved 2/2 images in ascendent order.

[8] M. S. Pattichis and A. C. Bovik, "Analyzing image structure by multidimensional frequency modulation," *IEEE Transactions on Pattern Analysis and Machine Intelligence*, vol. 29, no. 5, pp. 753–766, 2007.

[9] Victor Manuel Murray Herrera, "AM-FM methods for image and video processing," Ph.D. dissertation, University of New Mexico, 2008.

[10] M. Pattichis, J. Ramachandran, M. Wilson, C. Pattichis, and P. Soliz, "Optimal scanning, display, and segmentation of the international labor organization (ILO) X-ray images set for pneumoconiosis," in *IEEE Symposium on Computer-Based Medical Systems*, 2001, pp. 511–515.

[11] V. Murray, P. Rodriguez, and M. S. Pattichis, "Multi-scale AM-FM demodulation and reconstruction methods with improved accuracy," *accepted to the IEEE Trans. on Image Processing*, 2009.

[12] V. Murray, M. Pattichis, and P. Soliz, "New AM-FM analysis methods for retinal image characterization," in *Asilomar Conference on Signals, Systems and Computers*, 2008.

[13] J. P. Havlicek, "AM-FM image models," Ph.D. dissertation, The University of Texas at Austin, 1996.

[14] J. Havlicek, P. Tay, and A. Bovik, *Handbook of Image and Video Processing*. Elsevier Academic Press, 2005, ch. AM-FM Image Models: Fundamental Techniques and Emerging Trends, pp. 377–395.

[15] M. Pattichis, H. Muralldharan, C. Pattichis, and P. Soliz, "New image processing models for opacity image analysis in chest radiographs," in *IEEE Southwest Symposium on Image Analysis and Interpretation*, 7-9 April 2002, pp. 260–264.